Additive Manufacturing 24 (2018) 479–485

Contents lists available at ScienceDirect

Additive Manufacturing

journal homepage: www.elsevier.com/locate/addma

Full Length Article

Thermal conductivity of sintered copper samples prepared using 3D printing-compatible polymer composite filaments

Navid Dehdari Ebrahimi*, Y. Sungtaek Ju

Department of Mechanical and Aerospace Engineering, University of California, Los Angeles, CA, 90095, USA

ARTICLE INFO

Keywords:
3D printing
Copper
Metal-polymer composites
Oxidation
Sintering
Thermal conductivity

ABSTRACT

Metal-filled polymers containing micro-powders of highly conductive metals can serve as a starting material to fabricate complex metal structures using economic filament extrusion-based 3D printing and molding methods. We report our measurements of the thermal conductivity of copper samples prepared using these methods before and after a thermal treatment process. Sintering the samples at 980 °C leads to an order of magnitude improvement in thermal conductivity when compared with as-printed or as-molded samples. Thermal conductivity values of approximately 30 W/mK are achieved using commercially available polymer-copper composite filaments with a copper volume fraction of 0.4. Over-sintering the samples at 1080 °C further enhances the thermal conductivity by more than two folds, but it leads to uncontrolled shrinkage of the samples. The measured thermal conductivities show a modest decrease with increasing temperatures due to increased electron-phonon scattering rates. The experimental data agree well with the thermal conductivity models previously reported for sintered porous metal samples. The measured electrical conductivity, Young's modulus and yield strength of the present sintered samples are also reported.

1. Introduction

Polymers such as Polylactic Acid (PLA) and Acrylonitrile Butadiene Styrene (ABS) are some of the most widely used base materials for filament-based 3D printing. Recently, polymeric filaments blended with micro-powders of copper, bronze, aluminum, and other metals have become commercially available, enabling facile manufacture of 3D metal objects using inexpensive commercial 3D printers. By using high concentrations of thermally conductive metal particles, this approach is also promising for creating high-thermal conductivity components with complex 3D shapes. Hot pressing or post-processing, such as sintering at elevated temperatures, can be used to remove the polymeric binder and improve the thermal conductivity. The resulting porous structures are well-suited for diverse heat transfer and chemical applications where mechanical strength is of secondary importance, including but not limited to: advanced wick structures for heat pipes and vapor chambers [1–3]; textured surfaces for air-cooled heat exchangers [4,5]; catalysts in industrial chemical reactions such as hydrogen production [6]; energy storage and conversion [7]. Very few attempts, however, have so far been made to characterize the thermal conductivity and porosity of samples thus prepared.

The thermal conductivity of composites has been extensively studied in the past [8,9]. For a composite consisting of high-conductivity particles dispersed in a low-conductivity matrix, the contact resistance between the particles plays a major role in limiting heat conduction. For hot-pressed or sintered samples, Aivazov and Domashnev [10] suggested the following correlation for the effective thermal conductivity k_{eff}

$$\frac{k_{eff}}{k_m} = \frac{1-\varepsilon}{1+11\varepsilon^2} \tag{1}$$

where k_{m} is the thermal conductivity of the base metal and ε is the porosity. Alexander [11] and Bruggeman [12] proposed other correlations that account for the finite thermal conductivity of void gaps. Past experimental studies [13–18] showed that predictions from these models are in good agreement with the experimental data of sintered samples.

More recently, Laureto et al. [19] measured the thermal conductivity of various metal-polymer composites, including copper powders dispersed in a PLA matrix at volume concentrations similar to what is used in the present study. The measured thermal conductivity, however, was rather poor (< 2 W/m K). Although post-processing can improve the thermal conductivity of such 3D printed samples, the previous study did not explore such options.

In the present work, we report our measurement of the thermal, electrical and mechanical properties of metal samples prepared using PLA-copper composite filaments as the starting material. In Sec. 2, we describe our experimental setup and the procedure used to prepare the

* Corresponding author.
E-mail address: navid.dehdari@ucla.edu (N. Dehdari Ebrahimi).

https://doi.org/10.1016/j.addma.2018.10.025
Received 2 August 2018; Received in revised form 20 September 2018; Accepted 14 October 2018
Available online 16 October 2018

Table 1
3D printing settings.

Layer height (mm)	0.3
Shell thickness (mm)	0.5
Bottom/top thickness (mm)	0.5
Fill density (%)	100
Print speed (mm/s)	30
Hot end temperature (° C)	205
Bed temperature (° C)	50

samples. The results of our measurements are provided and discussed in Sec. 3. Our concluding remarks are presented in Sec. 4.

2. Experimental setup

2.1. Materials and sample fabrication

We use commercially available 3D printing filaments of PLA-copper composites (The Virtual Foundry, Inc.) to prepare samples for thermal conductivity measurements. The density of the filament and its copper volume fraction are measured to be 4.3 g/cm^3 and 0.4, respectively. The diameters of copper particles vary considerably, 32 ± 30 μm from SEM images (see Sec. 3).

Cylinders of diameter 2.56 cm and variable heights are prepared using a commercial 3D printer (Lulzbot Taz 6) with a 0.5 mm diameter extruder. The printing settings are listed in Table 1. Other samples are produced by molding. PLA-copper filament is heated to 250 °C on a hot plate and the softened mixture is poured into a mold and compressed at approximately 200 kPa (Fig. 1a) for 30 min. After the samples are allowed to cool down to the room temperature, the top and bottom surfaces are machined to yield a smooth surface for thermal conductivity measurements.

The samples are next sintered to remove the PLA binder and increase direct thermal contacts between copper particles. Prior to sintering, the samples are soaked in a solution of water, calcium sulfate and carbon (CSC). When dried, this solution forms an encapsulating layer around each sample, which in turn creates an anoxic environment during high-temperature sintering to help reduce oxidation [20,21]. The samples are next sintered in a benchtop furnace (Thermo Scientific Lindberg/Blue M Moldatherm). Two heating profiles (Fig. 1b) are used. In the second profile, the temperature is raised to slightly below the melting point of the copper for a short period of time to further increase the density of the samples. We refer to this step as over-sintering. The samples are quenched in water immediately after they are taken out of the furnace.

Some of the samples were prepared while injecting argon into the chamber at a flow rate of 12 l/min. This flow rate ensures that the gas inside the furnace is replaced every 30 s. Table 2 lists the bulk densities and copper volume fractions for different types of samples prepared using the procedures explained above. Bulk densities are calculated using two methods: direct measurement of mass and apparent volume and Archimedes method. The densities reported in Table 2 are the averaged values from the two methods. A weight scale (Adventurer Pro, Ohaus) with a resolution of 0.0001 g is used to measure the mass. The apparent volume of the samples is calculated by measuring the height and diameter of the cylinders with an uncertainty of 0.1 mm.

To measure the bulk density of the sintered samples using Archimedes method, we coat the samples with paraffin to avoid water diffusion into the micropores resulted from the PLA evaporation and weigh the immersed samples in water. Densities are then obtained using the following equation, assuming that the volume of the paraffin coating is negligible.

$$\rho_A = \frac{m_{dry}}{\Delta m_B}\rho_{water} \quad (2)$$

Here, m_{dry} is the mass of the dry sample before paraffin coating and Δm_B is the apparent mass difference due to buoyancy.

The volume fraction of the copper particles in non-sintered samples is calculated by assuming that the volume fraction of air voids is negligible, i.e. the samples are composed of copper and PLA matrix only. This is a valid assumption as Laureto et al. [19] observed less than 6% air void in their 3D printed samples using SEM imaging. Similarly, for sintered samples, we assume that the PLA matrix is fully evaporated, and the samples contain copper and air voids (see SEM images in Sec. 3).

From Table 2 we note that the density of the sintered samples is lower than that of the non-sintered samples due to PLA evaporation. We also observe that no significant increase in the density of molded samples is observed compared to the 3D printed samples for both non-sintered and sintered specimens.

2.2. Material properties measurement

The thermal conductivities of the samples are measured using a parallel-plate set up shown in Fig. 2. The setup consists of heated and

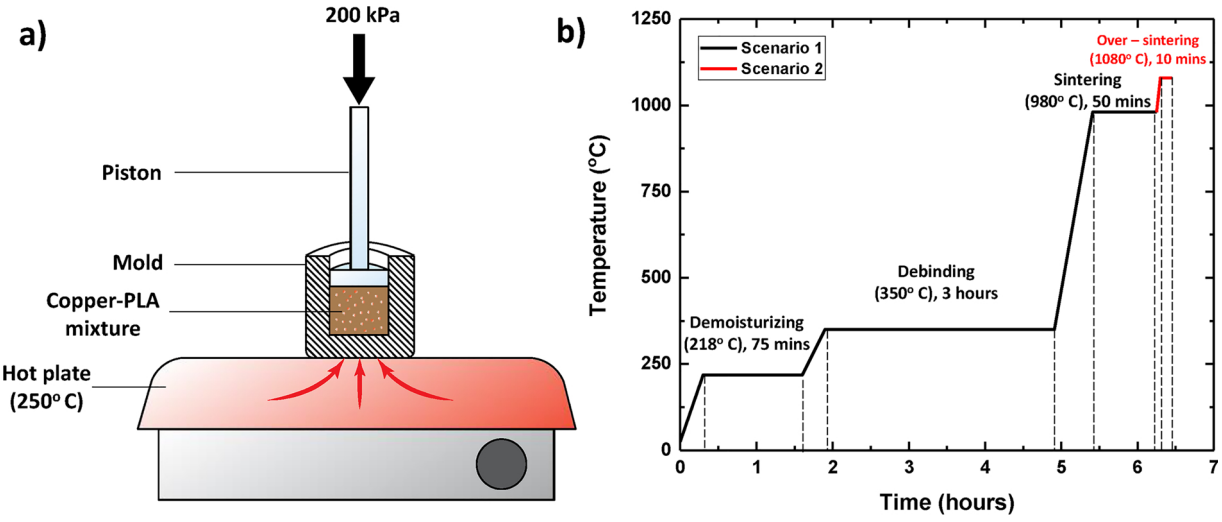

Fig. 1. a) Schematic of the molding process b) The heating profiles used for the sample preparation. In Demoisturizing step, water in the CSC is evaporated. Next, the temperature is increased to further evaporate PLA binder (Debinding step). Finally, the temperature is raised to 980 °C, where the actual sintering takes place. For the second heating profile, the over-sintering step (shown in red) is added. (For interpretation of the references to colour in this figure legend, the reader is referred to the web version of this article).

Table 2
Density and copper volume fraction of the different samples.

	Sample ID	Density ρ (direct measurement) (g/cm^3)	Density ρ (Archimedes method) (g/cm^3)	Average density $\bar{\rho}$ (g/cm^3)	Copper volume fraction φ_{Cu}	Average copper volume fraction $\bar{\varphi}_{Cu}$
non-sintered/ 3D printed	1	4.303	4.142	4.288	0.398	0.393
	2	4.341	4.390		0.403	
	3	4.130	4.426		0.376	
non-sintered/ molded	1	4.415	4.384	4.378	0.414	0.408
	2	4.558	4.356		0.431	
	3	4.144	4.412		0.378	
sintered/3D printed	1	3.800	3.832	3.751	0.427	0.423
	2	3.980	3.598		0.447	
	3	3.508	3.787		0.394	
sintered/molded	1	3.960	3.791	3.952	0.445	0.448
	2	4.000	3.941		0.449	
	3	3.991	4.028		0.448	
over-sintered/molded	1	5.595	5.581	5.588	0.629	0.629

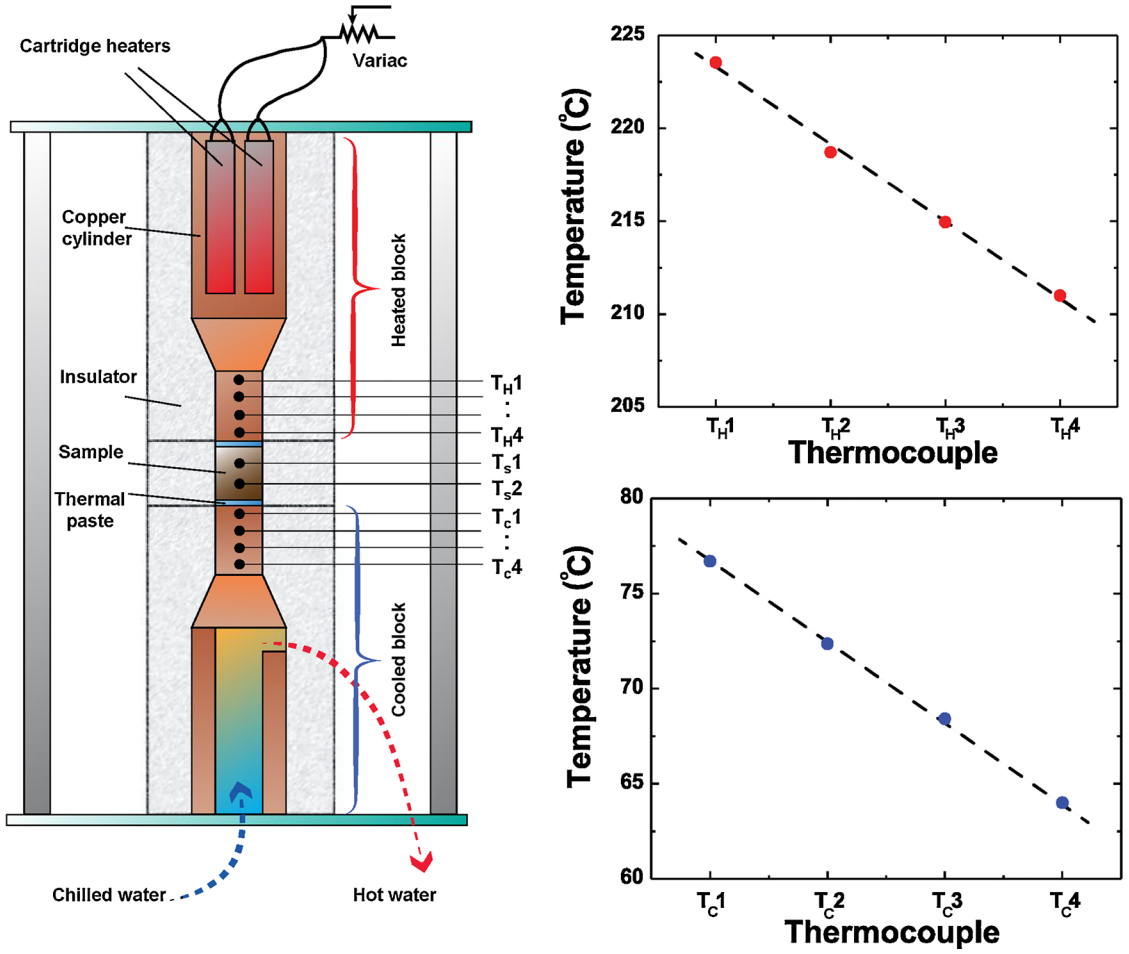

Fig. 2. Schematic of the thermal conductivity measurement setup. The two graphs on the right show representative thermocouple readings along the hot and cold blocks under steady state.

cooled cylindrical blocks, both made of copper. A sample is clamped between these two blocks for measurements at a loading pressure of 80 kPa. A thermal paste (Arctic Silver 5 AS5-3.5 G Thermal Paste) is applied between the contact surfaces of the sample and the two cylindrical blocks to reduce contact resistance.

Two cartridge heaters (OMEGA, CIR-20203/*, 200 W) are embedded in the heated block. The input power to the heaters is manually controlled using a variac. Chilled water (~20 °C) is circulated through the cold block to serve as the heat sink.

The cylindrical blocks are tapered close to the sample to form the core test section. This is meant to achieve a sufficiently high heat flux and to reduce the effects of heat loss from the heaters, especially through their power lines, on measurement accuracy.

Two arrays of four type-K thermocouples, each spaced 5 mm apart, are used to measure axial temperature gradients and hence axial conduction heat fluxes along the cylindrical blocks immediately before and after the sample. The uncertainty in the temperature readings is 0.2 °C. The entire setup is insulated using fiberglass to reduce heat loss and closely approximate a 1D heat conduction situation. The difference between heat transfer rates obtained from the two thermocouple arrays, which is a measure of heat loss across the side surfaces of the core test section, is less than 10%. The setup is allowed to reach steady state for

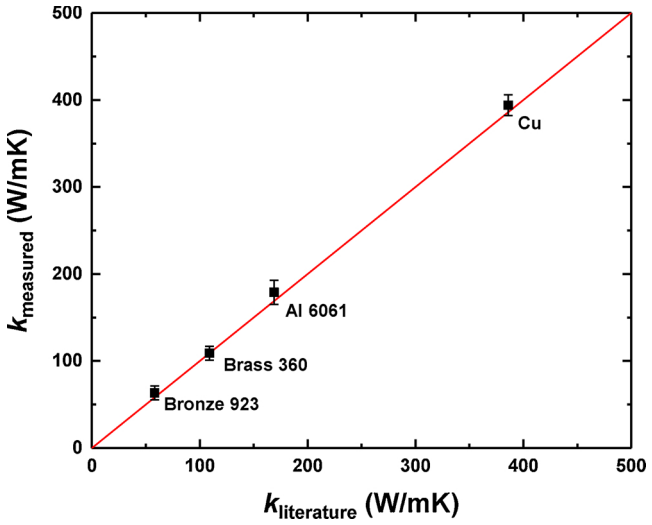

Fig. 3. The measured thermal conductivity of bulk metal samples using the setup described in Sec. 2 versus the reported values in the literature. The line is a line of slope 1.

approximately 1 h after any change in the heating power.

Two thermocouples are inserted into each sample through machined holes with 1 mm diameter that are spaced a known distance Δx_{sample} apart to determine the axial temperature gradient along the sample. The sample thermal conductivity is then computed as

$$k_{eff} = \frac{\bar{q}}{A\,\frac{T_{s1}-T_{s2}}{\Delta x_{sample}}} \quad (3)$$

where the average heat transfer rate along the two blocks is denoted as $\bar{q}$. The estimated uncertainty in the measured thermal conductivities is approximately 10% of the reported values. The main source of the error is the uncertainty in the axial heat flux, which arises from heat loss at the side surfaces of the core test section, instrument/calibration uncertainties and uncertainties in the measured geometric dimensions. Finite thermal resistance at the contact surfaces (the heating block to the sample and the sample to the cooled block) impedes axial heat conduction and leads to increased heat loss at the side surfaces of the core test section. To further validate our measurement setup, we measure the thermal conductivity of bulk metal samples and compare the results with the literature values in Fig. 3. The electrical conductivities of the sintered samples are measured using the four-probe method. A material testing machine (Instron 5800) is used to perform compression tests on the sintered samples.

3. Results and discussion

The measured thermal conductivities from five tested samples are listed in Table 3 along with the reported values from Laureto et al. [19] for the non-sintered sample.

From Table 3, we note that the thermal conductivity of the as-printed (non-sintered) sample is higher than the thermal conductivity of pure PLA (0.185 W/mK), but still much lower than that of pure copper (386 W/mK). Copper particles remain separated by PLA, which significantly impedes heat conduction. This is consistent with the results reported in Laureto et al. [19], which showed even lower thermal conductivity values due to lower metal contents. The classic models by Maxwell and Rayleigh tend to overestimate the thermal conductivity as they do not account for the thermal contact resistance between particles and the matrix. This is more problematic for smaller particles with higher surface-to-volume ratios [8]. The size of the copper particles used in [19] is smaller than the ones used in the present study (15 μm versus 32 μm).

Sintering the samples results in a considerable increase in the thermal conductivity as the PLA matrix is removed and copper particles form connected chains (Fig. 4) and hence highly conductive paths [24]. The 3D printed samples have slightly lower thermal conductivities than the molded samples. This is due in part to voids created as the 3D printing nozzle follows each vector path [19,25,26]. This is confirmed in the SEM images shown in Fig. 4a and b, where we observe more instances of large void (shown as dark areas) in the 3D printed sample (4a) compared with the molded sample (4b). We comment that optimization of the sintering conditions, which is challenging due to wide particle size distributions in commercial filaments, is beyond the scope of the present study.

Sintering the samples in an argon environment leads to only modest (approximately 10%) improvement in thermal conductivity. In contrast, the thermal conductivity of the over-sintered sample is considerably higher, almost by a factor of 2. The SEM image shown in Fig. 4c suggests that partial melting of copper particles leads to enlargement of particle-particle contact areas and reduction in air gaps in-between. This partial melting, however, also creates undesirable shrinkage in the samples. We observed approximately 30% reduction in volume after over-sintering at 1080 °C.

Thermal oxidation of copper during sintering is problematic because the resulting oxide layers have substantially lower thermal conductivities than that of copper. Past studies [27] observed the formation of almost 200 μm-thick oxide layers on fully exposed copper surfaces under conditions (1000 °C, 30 min) nominally similar to our sintering process.

To quantify the extent of copper oxidation in our sintering process, where the samples were encapsulated with thick layers of calcium sulfate and carbon, we perform EDX (energy dispersive x-ray spectroscopy) line scans across representative copper particles (Fig. 5). The focused ion beam (FIB) milling technique is used to cut through individual particles and expose their interiors for EDX scanning. For the samples sintered in the air atmosphere, we observe that an oxide shell of thickness approximately 1 μm was formed on the copper particles. No appreciable oxide shell of thickness above our resolution limit, estimated to be of the order of 0.3 μm, is observed for the samples sintered in the argon atmosphere. This is consistent with the higher thermal

Table 3
Measured thermal conductivity of sintered and non-sintered samples compared with model predictions.

	Density (g/cm^3)	Estimated porosity, 1-φ_{Cu}	Average thermal conductivity k^-_{eff} (W/mK)	Maxwell model [22] (W/mK)	Rayleigh model [23] (W/mK)	Aivazov & Domashnev [10] (W/mK)
3D printed / non-sintered	4.3	0.6	1.5	3.00	2.92	–
Molded / non-sintered	4.4	0.59	1.58	3.01	2.92	–
3D printed / non-sintered (Laureto et al. [19])	3.2	~ 0.75	0.44	1.99	1.99	–
3D printed / sintered in air	3.75	0.58	25.5	–	–	34.35
Molded / sintered in air	3.95	0.55	31	–	–	37.8
Molded / sintered in argon	3.95	0.55	34.2	–	–	37.8
Molded / over-sintered in air	5.6	0.38	81	–	–	92.3

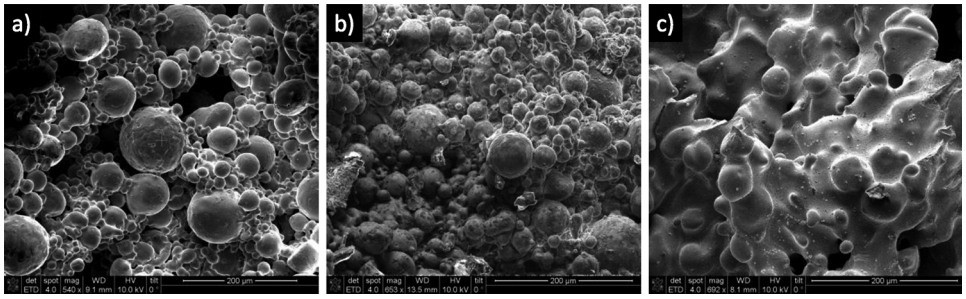

Fig. 4. The SEM images of the cross-sections of the samples after sintering: (a) 3D printed, (b) molded, and (c) over-sintered samples.

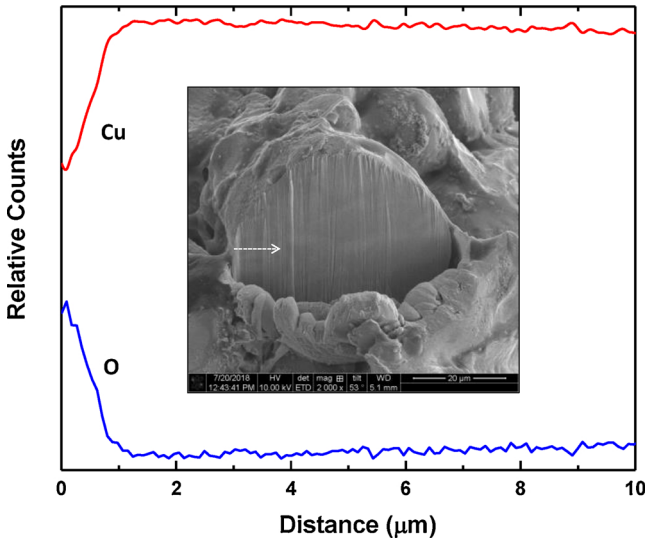

Fig. 5. EDX line scan (along the white arrow) from a copper particle of the sample sintered in the air. The inset is an SEM image of the copper particle, which was cut using the focused ion beam (FIB) technique to expose the interior. Background oxygen signals originated from a native oxide layer formed on the exposed surfaces during sample preparation and handling.

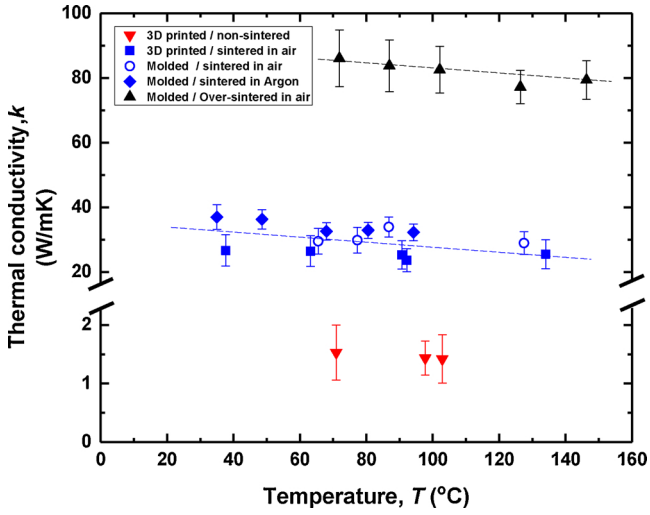

Fig. 7. Measured thermal conductivities as a function of the average temperature of the samples. The dashed lines represent the rate at which thermal conductivity of copper decreases with temperature. The error bars indicate the uncertainty in the measured values due to the heat loss, temperature reading fluctuations, and thermocouple position.

conductivities of the latter samples.

We next compare our experimental data with the previous data on sintered metal samples and model predictions in the literature. Fig. 6 shows the normalized thermal (6a) and electrical (6b) conductivities as a function of the sample porosity. Different samples from independent previous studies exhibit similar general trends, which are well captured by the models specifically developed for the thermal conductivity of sintered samples. The values obtained in this study agree reasonably well with the model predictions. The predicted value from one of the models [10] is also listed in Table 3.

Fig. 7 shows the same measured values listed in Table 3 as a function of the average sample temperature, $(T_{s1}+T_{s2})/2$. We observe that the thermal conductivity decreases with temperature at a rate of

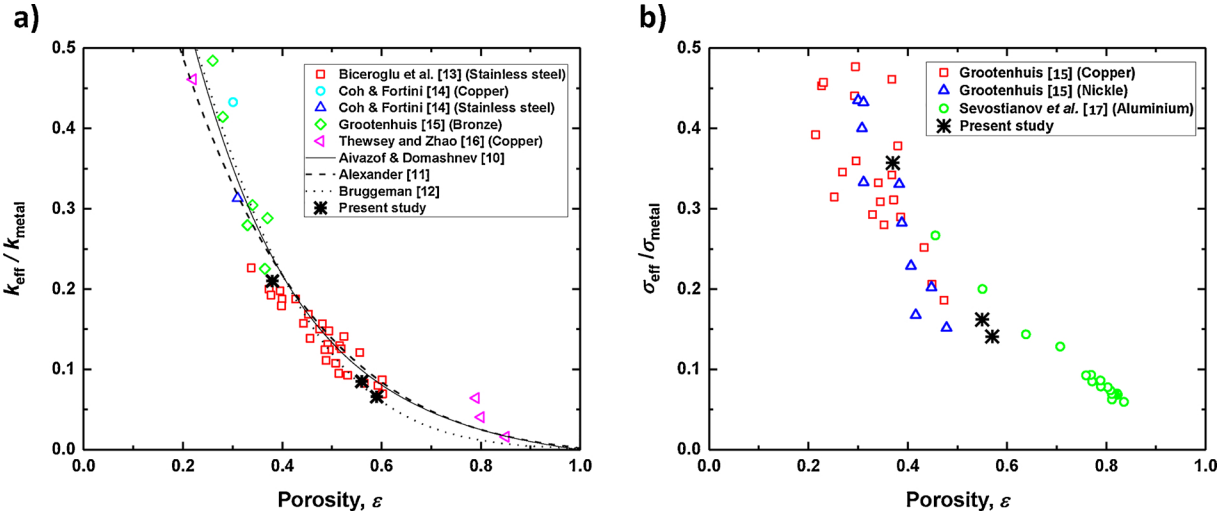

Fig. 6. a) Normalized thermal and b) electrical conductivities of sintered metal samples as a function of the porosity. The present results are shown as the asterisks.

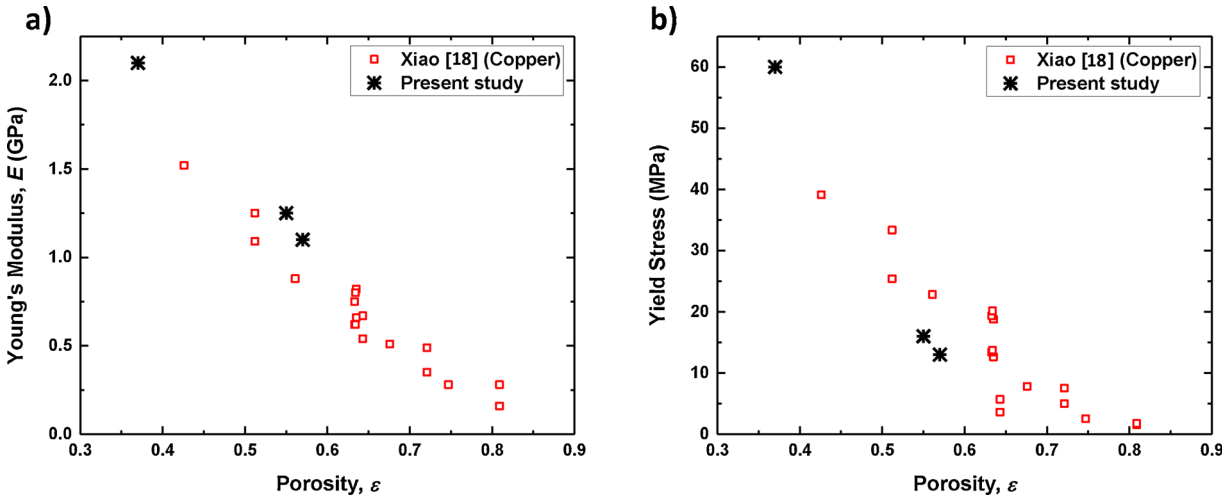

Fig. 8. a) Measured Young's modulus and b) yield stress of the sintered copper samples as a function of porosity.

approximately 0.075 W/mK^2. This is consistent with the temperature dependence of the thermal conductivity of pure copper [28], which is governed primarily by increased electron-phonon scattering rates at higher temperatures. This trend, however, does not apply to the non-sintered samples because the variation of thermal conductivity with temperature in these samples is mostly governed by the polymer matrix rather than the metal particles. In most non-crystalline polymers, the thermal conductivity does not vary significantly with temperature, with modest peaks at the glass transition temperature T_g (~ 60 °C for PLA) and gradually drops thereafter [29].

Unlike the thermal and electrical conductivities, the mechanical properties of sintered samples are known to depend strongly on manufacturing methods, particle attachment condition and the size and shape of particles. Large variations were observed in the yield stress and elastic modulus of sintered copper samples prepared using different methods such as the compressed vacuum sintering [30] and the lost-carbonate sintering method [18,31]. These variations might also arise from challenges in extracting these properties because porous metals often exhibit nonconventional stress-strain behavior [30]. We use the methods suggested in [18] to determine the Young's modulus and yield stress of our samples and show them in Fig. 8. Our results are consistent with the reported values in [18], where they used the lost-carbonate sintering method that is similar to the sintering approach adopted in the present study.

4. Conclusion

We report the experimentally measured thermal conductivity of metal samples prepared using filaments of polymer-copper composites as the starting material for 3D printing and molding. Post-thermal-processing of 3D printed polymer-copper composite samples at temperatures near 1000 °C significantly increases the thermal conductivity, to over 30 W/m K for samples with copper volume fractions of approximately 40%. The measured thermal and electrical conductivities agree with the previous literature values and the predictions from theoretical models developed for sintered metal samples. The thermal conductivity of the sintered samples exhibits a modest decrease with increasing temperatures, similar to the behavior of bulk copper. The measured Young's modulus and yield stress are consistent with the data reported in an independent study using samples prepared by a similar sintering process. The present study motivates further research and development efforts to develop promising methods of creating 3D metal samples of high thermal conductivities using economic polymeric filament-based 3D printing and molding methods.

References

[1] Y.S. Ju, et al., Planar vapor chamber with hybrid evaporator wicks for the thermal management of high-heat-flux and high-power optoelectronic devices, Int. J. Heat Mass Transf. 60 (May) (2013) 163–169.
[2] C. Ding, G. Soni, P. Bozorgi, B.D. Piorek, C.D. Meinhart, N.C. MacDonald, A flat heat pipe architecture based on nanostructured titania, J. Microelectromech. Syst. 19 (August 4) (2010) 878–884.
[3] J. Weibel, S. Garimella, J. Murthy, D. Altman, Design of Integrated Nanostructured Wicks for High-Performance Vapor Chambers, IEEE Trans. Compon. Packag. Manuf. Technol., 2011.
[4] S.W. Chang, T.-M. Liou, M.H. Lu, Heat transfer of rectangular narrow channel with two opposite scale-roughened walls, Int. J. Heat Mass Transf. 48 (September 19) (2005) 3921–3931.
[5] F. Zhou, I. Catton, A numerical investigation of turbulent flow and heat transfer in rectangular channels with elliptic scale-roughened walls, J. Heat Transf. 135 (June 8) (2013) 81901-81901–9.
[6] Y. Tang, W. Zhou, M. Pan, H. Chen, W. Liu, H. Yu, Porous copper fiber sintered felts: an innovative catalyst support of methanol steam reformer for hydrogen production, Int. J. Hydrog. Energy 33 (June 12) (2008) 2950–2956.
[7] Y. Li, Z.-Y. Fu, B.-L. Su, Hierarchically structured porous materials for energy conversion and storage, Adv. Funct. Mater. 22 (November 22) (2012) 4634–4667.
[8] K. Pietrak, T.S. Wisniewski, A review of models for effective thermal conductivity of composite materials, J. Power Technol. Wars. 95 (1) (2015) 14–24.
[9] R.I.P. Vachon, Thermal Conductivity of Heterogeneous Mixtures and Lunar Soils, (1973).
[10] M.I. Aivazov, I.A. Domashnev, Influence of porosity on the conductivity of hot-pressed titanium-nitride specimens, Powder Metall. Met. Ceram. 7 (9) (1968) 708–710.
[11] E.G. Alexander Jr., Structure–property Relationships in Heat Pipe Wicking Materials, (1972).
[12] D.A.G. Bruggeman, Dielectric constant and conductivity of mixtures of isotropic materials, Ann. Phys. Leipzig 24 (1935) 636–679.
[13] O. Biceroglu, A.S. Mujumdar, A.R.P. van Heiningen, W.J.M. Douglas, Thermal conductivity of sintered metal powders at room temperature, Lett. Heat Mass Transf. 3 (May 3) (1976) 183–191.
[14] J.C.Y. Koh, A. Fortini, Prediction of thermal conductivity and electrical resistivity of porous metallic materials, Int. J. Heat Mass Transf. 16 (November 11) (1973) 2013–2022.
[15] P. Grootenhuis, R.W. Powell, R.P. Tye, Thermal and electrical conductivity of porous metals made by powder metallurgy methods, Proc. Phys. Soc. Sect. B 65 (7) (1952) 502.
[16] D.J. Thewsey, Y.Y. Zhao, Thermal conductivity of porous copper manufactured by the lost carbonate sintering process, Phys. Status Solidi A 205 (May 5) (2008) 1126–1131.
[17] I. Sevostianov, J. Kováčik, F. Simančík, Elastic and electric properties of closed-cell aluminum foams: cross-property connection, Mater. Sci. Eng. A 420 (March 1) (2006) 87–99.
[18] Z. Xiao, Heat Transfer, Fluid Transport and Mechanical Properties of Porous Copper Manufactured by Lost Carbonate Sintering," Thesis, University of Liverpool, 2013.
[19] J. Laureto, J. Tomasi, J.A. King, J.M. Pearce, Thermal properties of 3-D printed polylactic acid-metal composites, Prog. Addit. Manuf. 2 (June 1–2) (2017) 57–71.
[20] O. Lame, D. Bellet, M. Di Michiel, D. Bouvard, Bulk observation of metal powder sintering by X-ray synchrotron microtomography, Acta Mater. 52 (February 4) (2004) 977–984.
[21] R.M. Anklekar, D.K. Agrawal, R. Roy, Microwave sintering and mechanical properties of PM copper steel, Powder Metall. 44 (October 4) (2001) 355–362.
[22] M. Levin, M. Miller, Maxwell a treatise on electricity and magnetism, Uspekhi Fiz. Nauk 135 (3) (1981) 425–440.

[23] Lord Rayleigh, LVI. On the influence of obstacles arranged in rectangular order upon the properties of a medium, Lond. Edinb. Dublin Philos. Mag. J. Sci. 34 (211) (1892) 481–502.
[24] R.S.P. Amit, Devpura Patrick, E. Phelan, Size effects on the thermal conductivity of polymers Laden with highly conductive filler particles, Microscale Thermophys. Eng. 5 (no. July 3) (2001) 177–189.
[25] B.M. Tymrak, M. Kreiger, J.M. Pearce, Mechanical properties of components fabricated with open-source 3-D printers under realistic environmental conditions, Mater. Des. 58 (June) (2014) 242–246.
[26] B. Wittbrodt, J.M. Pearce, The effects of PLA color on material properties of 3-D printed components, Addit. Manuf. 8 (October) (2015) 110–116.
[27] K. Mimura, J.-W. Lim, M. Isshiki, Y. Zhu, Q. Jiang, Brief review of oxidation kinetics of copper at 350 °C to 1050 °C, Metall. Mater. Trans. A 37 (April 4) (2006) 1231–1237.
[28] R.W. Powell, C.Y. Ho, P.E. Liley, Thermal conductivity of selected materials, Natl. Stand. Ref. Data Ser. - Natl. Bur. Stand. 8 (1966).
[29] P. Dashora, G. Gupta, On the temperature dependence of the thermal conductivity of linear amorphous polymers, Polymer 37 (January 2) (1996) 231–234.
[30] J.C. Qiao, Z.P. Xi, H.P. Tang, J.Y. Wang, J.L. Zhu, Compressive property and energy absorption of porous sintered fiber metals, Mater. Trans. 49 (December 12) (2008) 2919–2921.
[31] M.A. El-Hadek, S. Kaytbay, Mechanical and physical characterization of copper foam, Int. J. Mech. Mater. Des. 4 (March 1) (2008) 63–69.